THE JOURNAL OF PHYSICAL CHEMISTRY B
A JOURNAL OF THE AMERICAN CHEMICAL SOCIETY

pubs.acs.org/JPCB

Article

Molecular Rectifiers with a Very High Rectification Ratio Enabled by Oxidative Damage in Double-Stranded DNA

Abhishek Aggarwal, Supriyo Naskar, and Prabal K. Maiti*

Cite This: J. Phys. Chem. B 2022, 126, 4636−4646

Read Online

ACCESS | Metrics & More | Article Recommendations

ABSTRACT: In this work, we report a novel strategy to construct highly efficient molecular diodes using oxidatively damaged DNA molecules. Being exposed to several endogenous and exogenous events, DNA suffers from constant oxidative damage, leading to the oxidation of guanine to 8-oxoguanine (8oxoG). Here, we study the charge migration properties of native and oxidatively damaged DNA using a multiscale multiconfigurational methodology comprising molecular dynamics, density functional theory, and kinetic Monte Carlo simulations. We perform a comprehensive study to understand the effect of different concentrations and locations of 8oxoG in a dsDNA sequence on its charge-transport properties and find tunable rectifier properties having potential applications in molecular electronics such as molecular switches and molecular rectifiers. We also discover the negative differential resistance properties of the fully oxidized Drew−Dickerson sequence. The presence of 8oxoG guanine leads to the trapping of charge, thus operating as a charge sink, which reveals how oxidized guanine saves the rest of the genome from further oxidative damage.

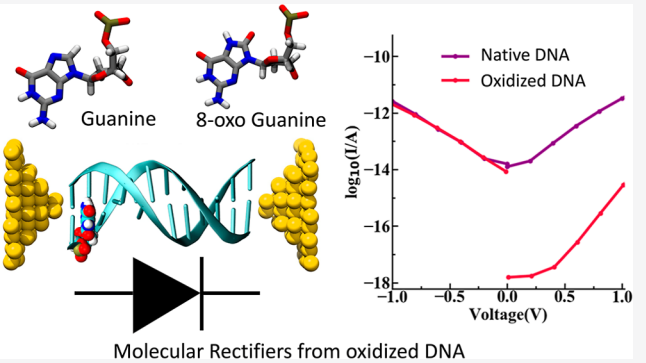

1. INTRODUCTION

Recent advances in the field of molecular electronics have revealed several fascinating phenomena of the quantum-mechanical tunneling regime, such as negative differential resistance (NDR),[1,2] molecular rectification,[3,4] thermoelectric effects,[5] and quantum interference.[5,6] The idea of molecular rectification was first anticipated by Aviram and Ratner in 1974.[7] Molecular rectifier devices display asymmetric current−voltage characteristics ($I-V$ characteristic curves) by favoring the charge current in one direction and disfavoring the current in the reverse direction. The ratio of the current in forward bias, that is, at a positive voltage $[I(V)]$ to the current in reverse bias; that is, at a negative voltage of the same magnitude, $[I(-V)]$ is defined as the rectification ratio (RR), which is generally used to determine the efficiency of a rectifier device.[8] A molecular device with a higher RR is considered to be an efficient rectifier. The RR can vary as the applied voltage increases across an asymmetric molecular system. A plethora of research works have been done to improve the RR of molecular devices.[3,5,9−13] The rectifying properties of molecules are usually induced using asymmetric molecule−electrode couplings,[14] using intercalations in molecular systems[9] or preparing asymmetric molecules.[3] A molecular diode with a high RR greater than 10 is difficult to form, and only a few works[3,4,15] have reported a RR > 10^2 to 10^3. In this work, we demonstrate a strategy to obtain molecular rectifiers with a record RR of as high as 6 orders of magnitude using oxidatively damaged double-stranded (ds) DNA molecules.

In the quest for miniaturization of electronic devices, dsDNA has emerged as a promising candidate to replace the conventional materials,[16−18] owing to its several unique properties, such as sequence-dependent extensibility,[19] self-assembly characteristics, and multiple charge transport (CT) mechanisms.[20,21] Charge migration in dsDNA is a vast research area leading to the development of several practical applications, from the construction of nanoscale biosensors to an enzymatic tool to detect damage in the genome.[16,18,21−31] dsDNA molecules inevitably suffer from oxidative damages by reactive oxidative species (ROS),[32,33] causing several DNA lesions and diseases such as cancer, and hold a huge biological significance.[33−37] The conversion of guanine to 8-oxoguanine (8oxoG) is one common defect produced by the oxidative damage of dsDNA.[32,38] These oxidative DNA repair and damages are often light-induced, and several efforts[39−42] have been made using quantum-mechanical

Received: February 25, 2022
Revised: June 5, 2022
Published: June 22, 2022

https://doi.org/10.1021/acs.jpcb.2c01371
J. Phys. Chem. B 2022, 126, 4636−4646

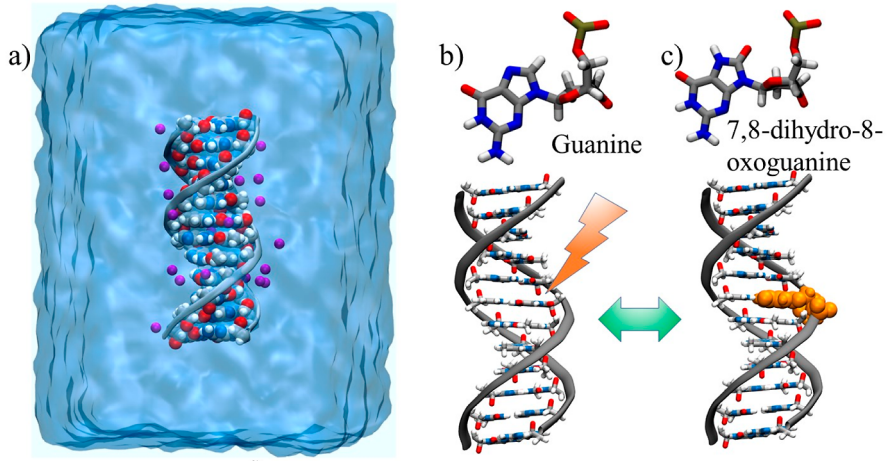

d) 12 base pair Poly-(GG)

GGGGGGGGGGGG CCCCCCCCCCCC Native DNA	GGGOOOOOOGGG CCCCCCCCCCCC Half-oxidized DNA	OOOOOOOOOOOO CCCCCCCCCCCC Full-oxidized DNA

e) Drew Dickerson Sequence

CGCGAATTCGCG GCGCTTAAGCGC Native DNA	COCGAATTCGCG GCGCTTAAGCGC Oxidation at 2nd Site CGCGAATTCGCO GCGCTTAAGCGC Oxidation at 12th Site	COCOAATTCGCG GCGCTTAAGCGC Double Oxidation	COCOAATTCGCG OCOCTTAAGCGC 4 Oxidations on Same Side COCOAATTCGCG GCGCTTAAOCOC 4 Oxidations on Opposite Side	COCOAATTCOCO OCOCTTAAOCOC All Guanines Oxidized

Figure 1. Details of the systems studied in this work. (a) Atomistic model of 12 bp oxidatively damaged dsDNA solvated in water during the MD simulations. For better clarity, water is shown as a continuous medium, rather than as an atomistic representation. (b) Atomic representation of guanine and 12 bp native dsDNA, which due to external factors oxidize to (c) 7,8-dihydro-8-oxoguanine (8oxoG), leading to oxidatively damaged dsDNA. (d,e) List of dsDNA sequences simulated in this study. The bold red O represents the replacement of guanine with 8oxoG.

calculations to understand these UV-induced charge-transfer processes in dsDNA components.

An increasing body of works has suggested that the presence of 8oxoG in DNA sequences acts as a hole sink, which biologically prevents the rest of the genome from further damage.[43,44] In this context, Burrows and co-workers[41,45,46] have done a tremendous amount of work to understand the mechanistic chemistry of guanine oxidation using free radical oxidants that play a huge role in cellular chemistry and highlight the self-repair property of 8oxoG containing DNA fragments.[41] A number of studies exist in the literature which aim to understand the molecular and electronic structures of oxidatively damaged dsDNA,[45−50] but none of them provides an account for the charge dynamics in oxidized dsDNA. This makes the study of CT in oxidatively damaged dsDNA immensely important. Through this work, our aim is to enhance the fundamental understanding behind the CT mechanism in oxidized dsDNA, which helps to understand the physics behind several interesting physical phenomena prevalent in nucleic acid systems, namely, rectification and NDR. Here, we reveal the rectifying properties of oxidatively damaged dsDNA molecules with a giant RR as high as 10^6. Thus, we present a novel strategy to fabricate molecular rectifiers using oxidatively damaged dsDNA molecules, pushing forward the ever-developing field of molecular electronics.

Using a multiscale multiconfigurational methodology involving atomistic MD simulations, quantum-mechanical density functional theory (DFT) calculations, and kinetic Monte Carlo (KMC) simulations, we study the hole migration phenomena in different 12 base pairs (bp) of native and 8oxoG-containing dsDNA sequences. By varying the concentration and location of 8oxoG in the Drew−Dickerson sequence, we report a RR of as high as 6 orders of magnitude. In the next section, we describe the multiscale multiconfigurational methodology employed to obtain the CT properties of various nucleic acid systems in this study. This methodology has been employed in several works[18,20,51−54] and aided in revealing several important aspects of CT in DNA systems.

2. METHODOLOGY

2.1. MD Simulation Details. To understand the variations of CT properties in a dsDNA sequence when a guanine is replaced by 8oxoG, we first simulate various biologically relevant dsDNA sequences for 100 ns using all-atomistic MD simulations using the AMBER18 software package,[55] as shown in Figure 1a−c. We study a 12 bp long poly-G sequence as an extreme case where all and half of the guanine gets oxidized Figure 1d. To study the effect of different concentrations and locations of 8oxoG, we simulate a Drew−Dickerson sequence, oxidized in various manners, as shown in Figure 1e. Such controlled oxidation of guanines in dsDNA has been done in various in vitro works to study their various biological aspects.[56,57] We build bare dsDNA in the B-form for 12 bp poly-G [d-(GGGGGGGGGGGG)] and Drew−Dickerson sequences [d-(CGCGAATTCGCG)] using the nucleic acid

https://doi.org/10.1021/acs.jpcb.2c01371
J. Phys. Chem. B 2022, 126, 4636−4646

builder (NAB)[58] tool. The oxidized guanine molecule is prepared using the parameters provided in the work by Miller et al.[59] We then use the xleap module of the AMBERTOOLS17[58] to solvate each complex in a large rectangular box, ensuring a 15 Å solvation shell around the dsDNA molecule in each direction molecule using the TIP3P[60] water model. Charge neutrality of the simulation box is maintained by adding appropriate numbers of Na^+ and Cl^- ions, for which Joung/Cheatham ion parameters[61] are used.

The system is then energy-minimized using the steepest descent method for 1000 steps, followed by 2000 steps of the conjugate gradient method, keeping a strong harmonic restraint of a force constant of 500 kcal mol^{-1} $Å^{-2}$ on dsDNA to allow the water molecules to equilibrate. Then, the dsDNA is slowly released into the water by reducing the harmonic restraint on it from 20 to 0 kcal mol^{-1} $Å^{-2}$ in 5 cycles of steepest descent minimization of 1000 steps each. After energy minimization, the system is slowly heated to reach a temperature of 300 K in 40 ps at a constant pressure of 1 bar. To control the temperature, we use the Langevin thermostat, with a collision frequency constant of 2.0 ps^{-1}. The particle mesh Ewald method[62] (PME) is used to calculate electrostatic interactions. A long-range cutoff of 10 Å was used for nonbonding interactions during the MD simulations. The NVT production run is then performed at a temperature of 300 K and pressure of 1 bar for 100 ns. We use the AMBER ff99bsc0 and OL15 force fields for modeling dsDNA molecules. The force-field parameters of 8oxoG are adapted from the study by Miller et al.[59] Bonds involving hydrogen atoms are constrained using the SHAKE algorithm which allowed the use of a 2 fs time step. The PMEMD module of the AMBER18[58] software is used for performing the MD simulations.

2.2. Hopping Transport Calculations. In this work, the semiclassical Marcus−Hush formalism[20,63] is used to obtain the $I-V$ characteristics of the dsDNA system. In this theory, CT is described as incoherent hopping of charge carriers between charge hopping sites. Several previous theoretical and experimental studies have shown that CT in dsDNA systems is mediated through strong $\pi-\pi$ stacking of nucleobases.[18,20,22,64] Thus, we use DNA nucleobases as hopping sites in this work by replacing the DNA backbone atoms with hydrogen atoms for further calculations and optimizations. We use the nearest-neighbor hopping model where a charge present at any nucleobase other than the terminal bases has five available sites to hop to, consisting of four hopping sites from two adjacent base pairs and the complementary base of the present site.

In Marcus−Hush formalism, the charge hopping rate ω_{ik} from the charge hopping site, i, to the hopping site, k, is given by[20,63]

$$\omega_{ik} = \frac{2\pi|J_{ik}|^2}{h}\sqrt{\frac{\pi}{\lambda k_B T}}\exp[-\frac{(\Delta G_{ik} - \lambda)^2}{4\lambda k_B T} \quad (1)$$

]where J_{ik} is the electronic coupling, also called the transfer integral, defined as

$$J_{ik} = <\Psi^i|H_{ik}|\Psi^k> \quad (2)$$

Here, Ψ^i and Ψ^k are diabatic wave functions localized on the sites i and k, respectively. H_{ik} is the Hamiltonian for the two-site system between which the charge transfer takes place. λ is the reorganization energy. ΔG_{ik} is the free energy difference (also known as site energy difference) between the two sites, h is Planck's constant, k_B is the Boltzmann constant, and T is the absolute temperature.

Previous studies have shown that the CT between two nucleobases of dsDNA molecules is strongly dependent on their relative positions and orientations.[20,42] In our work, the electronic couplings between all possible nearest-neighbor charge hopping base pairs are computed for 100 different nucleic acid configurations sampled from MD simulations to account for the effect of dynamic disorder arising due to the thermal fluctuations. These 100 different MD-simulated snapshots have been taken from the last 4 ns of the 200 ns-long MD simulation. To ensure that these configurations are not correlated with each other, we take the DNA configurations periodically keeping a time difference of 40 ps, which is higher than the correlation time of the base pair dynamics.[20] We then compute the electronic coupling for each possible hopping between different nucleobases for each chosen configuration using DFT and present the average $I-V$ characteristics in all the graphs.

The reorganization energy, λ_{ik}, has two parts: inner-sphere reorganization energy and outer-sphere reorganization energy. The inner-sphere reorganization energy considers the change in the nuclear degrees of freedom when the charge transfer takes place between one charge hopping site to another. This is defined as

$$\lambda_{ik}^{int} = U_i^{nC} - U_i^{nN} + U_k^{cN} - \quad U_k^{cC} \quad (3)$$

U_i^{nC} (U_i^{cN}) is the internal energy of a neutral (charged) base in charged (neutral) state geometry.U_i^{nN} (U_i^{cC}) is the internal energy of a neutral (charged) base in neutral (charged)-state geometry.

To compute the four-point internal energy values (U_i^{nN}, U_i^{cN}, U_i^{nC}, and U_i^{cC}) of eq 3, the isolated charge hopping sites are first optimized to obtain the charged and neutral geometries. Subsequently, the single-point energies of these configurations are computed in the charged and neutral states using the Gaussian09 software package, which can be incorporated in eq 3 to obtain the internal reorganization energy values. The reorganization of the environment as the charge transfer occurs is considered using the outer-sphere reorganization. This has been taken as a parameter (0 eV) in our calculations as the surrounding conditions for both native and oxidized dsDNA are the same for all the calculations. It is noteworthy to mention here that the reorganization energy computed using this approach does not account for the interaction between stacked nucleobases in different charged states, which may affect the reorganization energy between two nucleobases to some extent.

The total free energy difference between two hopping sites also consists of two parts: internal site energy difference and external energy difference. ΔG_{ik}^{ext} is the contribution due to the external electric field, taken as the potential difference between the two hopping sites in our calculations. We take uniform distribution of potential between the base pairs; that is, consecutive base pairs will have a potential difference of $[V/(N-1)]$, while bases of the same pairs will have zero potential difference, that is,

https://doi.org/10.1021/acs.jpcb.2c01371
J. Phys. Chem. B 2022, 126, 4636−4646

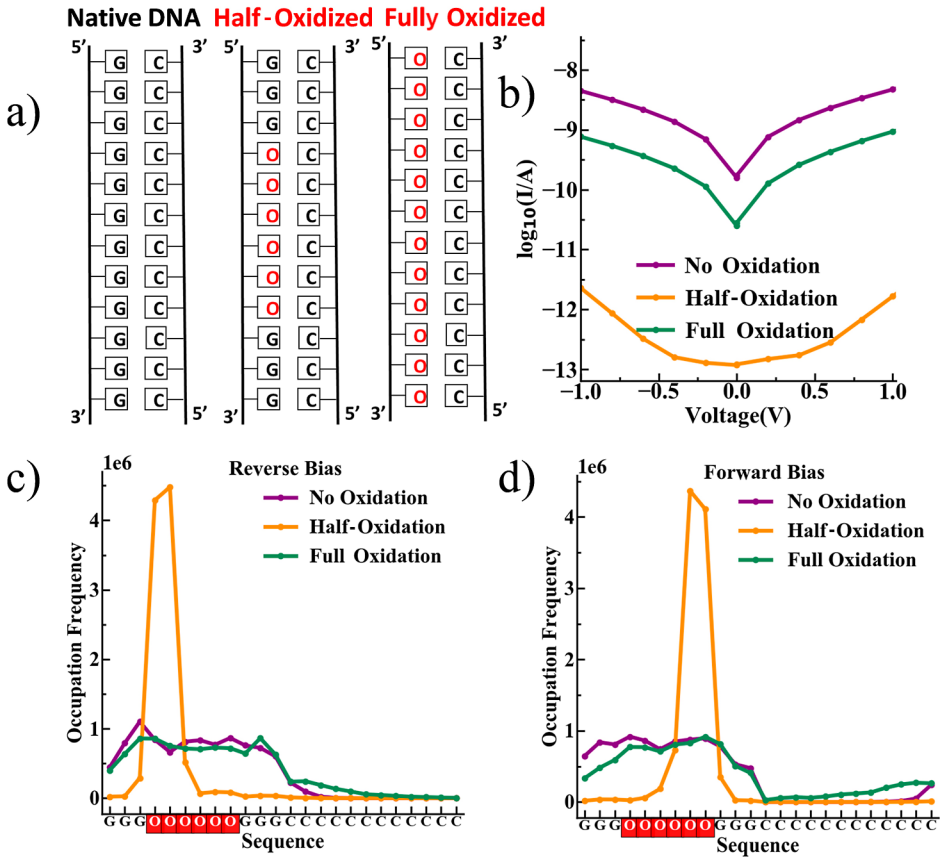

Figure 2. (a) Schematic representation showing the oxidation of half and all guanines of the 12 bp poly-(G) sequence. (b) Average $I-V$ characteristics averaged over 100 morphologies of the native and oxidized poly-(G) DNA sequence computed using multiscale methodology. (c) Occupation frequency of the hole at different nucleobases of dsDNA under (c) reverse bias and (d) forward bias. Clearly, 8oxoG acts as a bottleneck for CT in half-oxidized dsDNA, explaining the $I-V$ characteristics obtained in (b).

$$\Delta G_{ik}^{\text{ext}} = \begin{cases} \dfrac{V}{N-1}, & \text{for consecutive bases along the helical axis of DNA along positive volt} \\ 0, & \text{for base pairs at the same level along helical axis} \\ -\dfrac{V}{N-1}, & \text{for consecutive bases along the helical axis of DNA or along negative volt.} \end{cases} \tag{4}$$

N is the number of base pairs.

However,

$$\Delta G_{ik}^{\text{int}} = U_i^{\text{cC}} - U_i^{\text{nN}} + U_k^{\text{cC}} - U_k^{\text{nN}} \tag{5}$$

where $U_i^{\text{cC}}(U_i^{\text{nN}})$ is the internal energy of the base in the charged (neutral) state and geometry.

The calculation of transfer integrals and reorganization energies is performed using DFT, which has been carried out at the M062X/6-31g(d) functional level of theory using the Gaussian09 software package. The effect of solvation arising due to the surrounding water medium of the base pairs is considered using the polarizable continuum model[65] (PCM) in this work. We have used the integral equation formalism PCM (IEFPCM) version of the PCM for the calculations. It is noteworthy to mention here that explicit representation of the surrounding environment has also been done using quantum mechanics/molecular mechanics methods in the previous CT studies of DNA.[66,67] However, since both the native and oxidized dsDNA are immersed in a charge-neutral TIP3P water box of similar dimensions, their environment is similar.[43] Thus, changing the method of the representative external environment should not drastically affect the relative CT properties of native and oxidized dsDNA. Therefore, we use an implicit solvation method which has been demonstrated to approximate the DNA environment with sufficient accuracy in previous DNA CT works.[20,68,69] The VOTCA-CTP[54] software package is used to calculate the transfer integral values for all possible base pairs.

2.3. Kinetic Monte Carlo. Once we obtain all the hopping rates, we employ the KMC algorithm to simulate the charge dynamics of the system by solving the master equation containing the probabilities of a charge hopping site to hold charge. In this scheme, initially, a unit charge is assigned to a random hopping site i, and this instant is taken as the initial time, that is, $t = 0$. The waiting time is then computed using the following relation

$$\tau = -\omega_i^{-1}\ln(r_1) \tag{6}$$

Here, $\omega_i = \Sigma_{k=1}^{N}\omega_{ik}$ is the sum of all the hopping rates for the sites available for charge present at site i to hop, n is the number of charge hopping sites available for charge at site i, r_1 represents a uniform random number between 0 and 1, and k is the index for the available sites for hopping. Once the waiting time is calculated, the total time is then updated as $t = t + \tau$. To decide the site to which the charge has to hop to, the j value for which $\frac{\Sigma_k\omega_{ik}}{\omega} \leq r_2$ is largest and r_2 are chosen, where r_2

https://doi.org/10.1021/acs.jpcb.2c01371
J. Phys. Chem. B 2022, 126, 4636−4646

is another uniform random number between 0 and 1. The above condition ensures that the site k is chosen with probability $\frac{\omega_{ik}}{\omega}$. After this, the position of the charge is updated and the above process is repeated, providing the probabilities for each site. The current is then found using the following formula

$$I_{bp} = -e\left[\sum_i (P_{b_1}\omega_{b_1 i} - P_i\omega_{ib_1}) + \sum_i (P_{b_2}\omega_{b_2 i} - P_i\omega_{ib_2})\right] \quad (7)$$

Here, e is the unit electric charge, i stands for all the possible hopping sites which are in the direction of flow of current, and b_1 and b_2 are the base stacks of the base pair bp. Hence, the mean current is average over all base pairs, $I = \langle I_{bp} \rangle$.

Thus, our work employs a multiscale methodology to compute the CT properties of dsDNA molecules, which can be summarized as follows. We first perform a 200 ns-long MD simulation to obtain the atomic morphologies of dsDNA systems under aqueous conditions. From the last 4 ns of this simulation, we choose 100 morphologies (atomic coordinates) of the full dsDNA system. For each of this dsDNA morphology, we then remove the backbone atoms and add hydrogen atoms to complete the nucleobase valency. Thus, at this stage, we have 100 different sets of arrangements of a ladder-like structure of nucleobases between which the charge can hop. After that, we employ the DFT method to compute the hopping rate between the nearest-neighbor nucleobase pairs. The Hamiltonian of the two-site systems and the diabatic wave functions of the individual nucleobases mentioned in eq 2 are computed using these DFT calculations to obtain the electronic coupling values. Once the hopping rates for each possible charge hopping combination for each of the 100 morphologies is obtained using eq 1, we then use KMC simulations to obtain the charge dynamics of each morphology. Thus, we have 100 different $I-V$ characteristics for each studied dsDNA sequence. We then present the average of the $I-V$ characteristics for these 100 morphologies in the Results section.

3. RESULTS

We have studied the 12 bp poly-G dsDNA sequence by oxidizing all the guanine bases of the DNA chain in one case while oxidizing only the middle half of the sequence in the other case, as shown in Figure 2a. In this dsDNA sequence, we find that the native dsDNA exhibits the highest conductance relative to the oxidized dsDNA, while fully oxidized dsDNA shows higher conductance than half-oxidized dsDNA. This can be explained based on the charge dynamics in different DNA sequences (Figure 2c,d). As shown in Figure 2c,d, the charge gets trapped in the half-oxidized DNA at the point where the charge must hop between the oxidized and the native guanine base. However, for a native dsDNA or a fully oxidized DNA, such consecutive sequence mismatch is not present. It is precisely the emergence of this charge trapping in 8oxoG bases what explains, from a molecular point of view, the lower conductivity in half-oxidized poly-G dsDNA. Indeed, such trapping of holes at the 8oxoG sites has been reported earlier and has found a huge biological significance.[70] Based on experimental evidence, it has been demonstrated that the 8oxoG in the dsDNA sequence acts as a hole sink and saves the rest of the genome from further oxidative damage.[71] Our comprehensive analysis based on KMC simulations shows that the hole indeed gets trapped at the 8oxoG sites, giving rise to the concomitant effect of lower conductivity in oxidized DNA.

The energetics of 8oxoG and native guanine bases are largely responsible for the trapping of charge in oxidized dsDNA. To verify this, we have computed and compared the reorganization energy and the site energy differences of both guanine and 8oxoG with other nucleobases using the M062X level of theory using the 6-31g(d) basis set. We find that 8oxoG requires significantly higher reorganization energies and site energy differences to hop to other nucleobases, compared to that required for the native guanine for the same (Table 1). This

Table 1. Reorganization Energy and Site Energy Difference of Guanine and 8oxoG to Different Nucleobases for Different Basis Sets

		to A	to T	to C	to G	to O
basis set: 6-31 g(d)						
reorganization energy (in eV)	from G	0.615	0.595	0.502	0.684	0.678
	from O	0.64	0.62	0.527	0.709	0.703
site energy difference (in eV)	from G	−0.408	−0.774	0.769	0.0	0.355
	from O	−0.763	1.129	−1.124	−0.355	0.0
basis set: 6-31 g(d,p)						
reorganization energy (in eV)	from G	0.57	0.59	0.49	0.66	0.66
	from O	0.60	0.62	0.52	0.687	0.686
site energy difference (in eV)	from G	−0.41	−0.78	0.78	0.0	0.35
	from O	−0.77	1.13	−1.13	−0.35	0.0
basis set: 6-311++g(d,p)						
reorganization energy (in eV)	from G	0.56	0.61	0.52	0.66	0.67
	from O	0.59	0.64	0.55	0.69	0.70
site energy difference (in eV)	from G	−0.38	−0.73	0.77	0.0	0.32
	from O	−0.7	1.05	−1.1	−0.32	0.0
basis set: cc-PVTZ						
reorganization energy (in eV)	from G	0.58	0.61	0.52	0.66	0.67
	from O	0.61	0.64	0.55	0.69	0.70
site energy difference (in eV)	from G	−0.39	−0.77	0.8	0.0	0.33
	from O	−0.72	1.11	−1.13	−0.33	0.0
basis set: aug-cc-PVDZ						
reorganization energy (in eV)	from G	0.54	0.58	0.50	0.63	0.64
	from O	0.59	0.61	0.53	0.67	0.67
site energy difference (in eV)	from G	−0.38	−0.74	0.78	0.0	0.32
	from O	−0.70	1.06	−1.1	−0.32	0.0

energy difference reduces the probability of hopping of oxidized guanine, and hence, the charge gets trapped. To make sure that this observation is not an artifact of the basis sets used for the calculation of the energies, we use different basis sets as shown in Table 1 and find that the relative trend remains the same for the oxidized and native guanine molecules.

Having built a thorough understanding of the charge dynamics and energetics in native and oxidized dsDNA, we then ask the question of whether this knowledge can be used for molecular electronic applications. For this, we study the Drew−Dickerson dsDNA sequence and replace the guanine nucleobases at different locations and concentrations, as

https://doi.org/10.1021/acs.jpcb.2c01371
J. Phys. Chem. B 2022, 126, 4636−4646

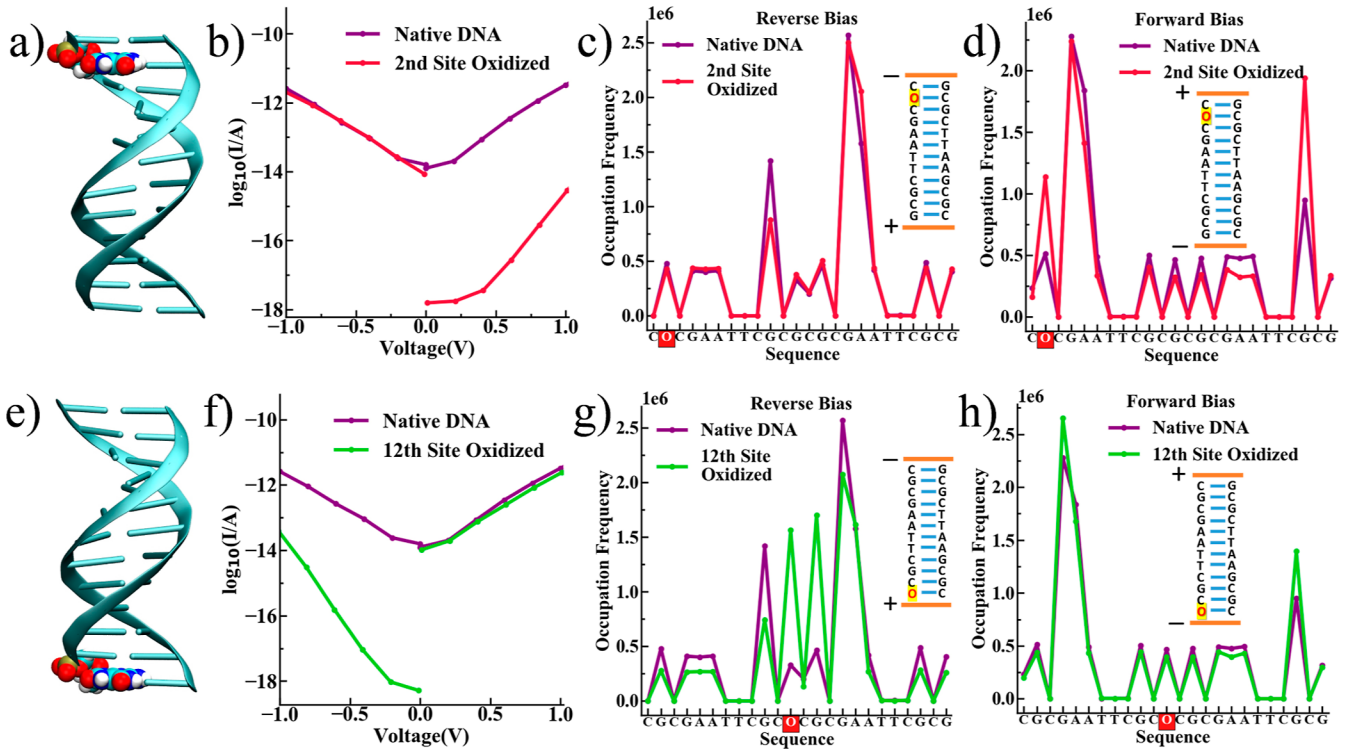

Figure 3. Effect of single guanine oxidation on CT properties of dsDNA. (a) 3-D structure of the Drew−Dickerson dsDNA sequence oxidized at the second site. 8oxoG is shown in the van der Waals (VDW) representation. (b) $I-V$ characteristics of the native Drew−Dickerson sequence compared to that of oxidized dsDNA with guanine at the 2nd site from the 5′ end replaced with 8oxoG. The occupation frequency of the charge during the KMC simulations for (c) reverse bias and (d) forward bias. Clearly, a sharp increase at the 8oxoG site is seen in the oxidized guanine in the forward bias at 8oxoG, giving rise to rectifying behavior of the molecule. The guanines replaced with 8oxoG are highlighted in red on the x-axis of the curves. (e) 3-D structure of the Drew−Dickerson dsDNA sequence oxidized at the 12th site. (f) $I-V$ characteristics of the native Drew−Dickerson sequence and that oxidized with the guanine at the 12th site from the 5′ end of dsDNA replaced with 8oxoG. The occupation frequency of the charge during the KMC simulations for (g) reverse bias and (h) forward bias.

explained in Figure 1e. We will now discuss the feasibility of 8oxoG to construct molecular rectifiers using Drew−Dickerson dsDNA as a case study.

In Figure 3, we first study the effect of oxidation of a single guanine nucleobase at different locations in Drew−Dickerson dsDNA. In one case, we replace the second nucleobase from the 5′ end of dsDNA with 8oxoG (Figure 3a), while in the other case, the nucleobase at the 12th site is replaced (Figure 3e). Figure 3b,f shows the comparison of $I-V$ characteristics of native dsDNA with dsDNA oxidized at the 2nd and 12th sites, respectively. We find strong rectification behavior in both the cases. While the dsDNA oxidized at the 2nd site shows 3 orders of magnitude lower conductance (RR = 1.4×10^{-3}) in forward bias, a 12th-site oxidation in dsDNA leads to similar dip in conductance in reverse bias (RR = 61.2). It is fascinating to note here that oxidation in only a single guanine base of the whole sequence leads to such drastic changes. The decrease in the conductance certainly comes from the charge dynamics and energetics of nucleobases, which is related to the hopping rates near the 8oxoG bases. In Figures 3c,d,we compare the charge dynamics in the second-site oxidized dsDNA and native dsDNA for both forward and reverse biases. While the probability of finding the charge at each site is similar in reverse bias (Figure 3c), there is an uptick in the charge occurrence at 8oxoG in forward bias (Figure 3d). This is because in the case of oxidation at the second site, the oxidation site is closer to the positive electrode in forward bias, causing a disruption in the flow of holes through the dsDNA. This increased occupation leads to a decrease in conductance in second-site oxidation in forward bias. Similarly, for 12th site oxidation, as the oxidized site is closer to the positive electrode in reverse bias, the occupation frequency of charge is higher at 8oxoG in reverse bias (Figure 3g), leading to lesser conductance in the reverse bias configuration. In the forward bias, the occupation frequency graph is similar to that of native dsDNA (Figure 3h), leading to a strong overall rectification behavior in the circuit. Thus, by varying the position of oxidation in dsDNA, one can obtain direction-dependent rectification properties in single-molecular circuits made up of dsDNA molecules.

To further check the effect of concentration of oxidation on dsDNA CT properties, we replace the two guanine bases near the 5′ end of one strand with 8oxoG (Figure 4a). Like the single-oxidation case, upon inspecting the $I-V$ characteristics, one can immediately observe a very strong rectification behavior in the oxidized dsDNA sequence with a high RR of around 6 orders of magnitude at 1 V (RR = $7.8 \times 10^{-}6$). This RR is computed as the ratio of current at +1 V (in forward bias) to the current at −1 V (in reverse bias). According to the results shown in Figure 4b

$$I(+1\ \mathrm{V}) = 3.25 \times 10^{-18}\ \mathrm{A} \tag{8}$$

$$I(-1\ \mathrm{V}) = 0.4 \times 10^{-12}\ \mathrm{A} \tag{9}$$

$$\mathrm{RR} = \frac{I(+1\ \mathrm{V})}{I(-1\ \mathrm{V})} = 7.8 \times 10^{-6} \tag{10}$$

https://doi.org/10.1021/acs.jpcb.2c01371
J. Phys. Chem. B 2022, 126, 4636−4646

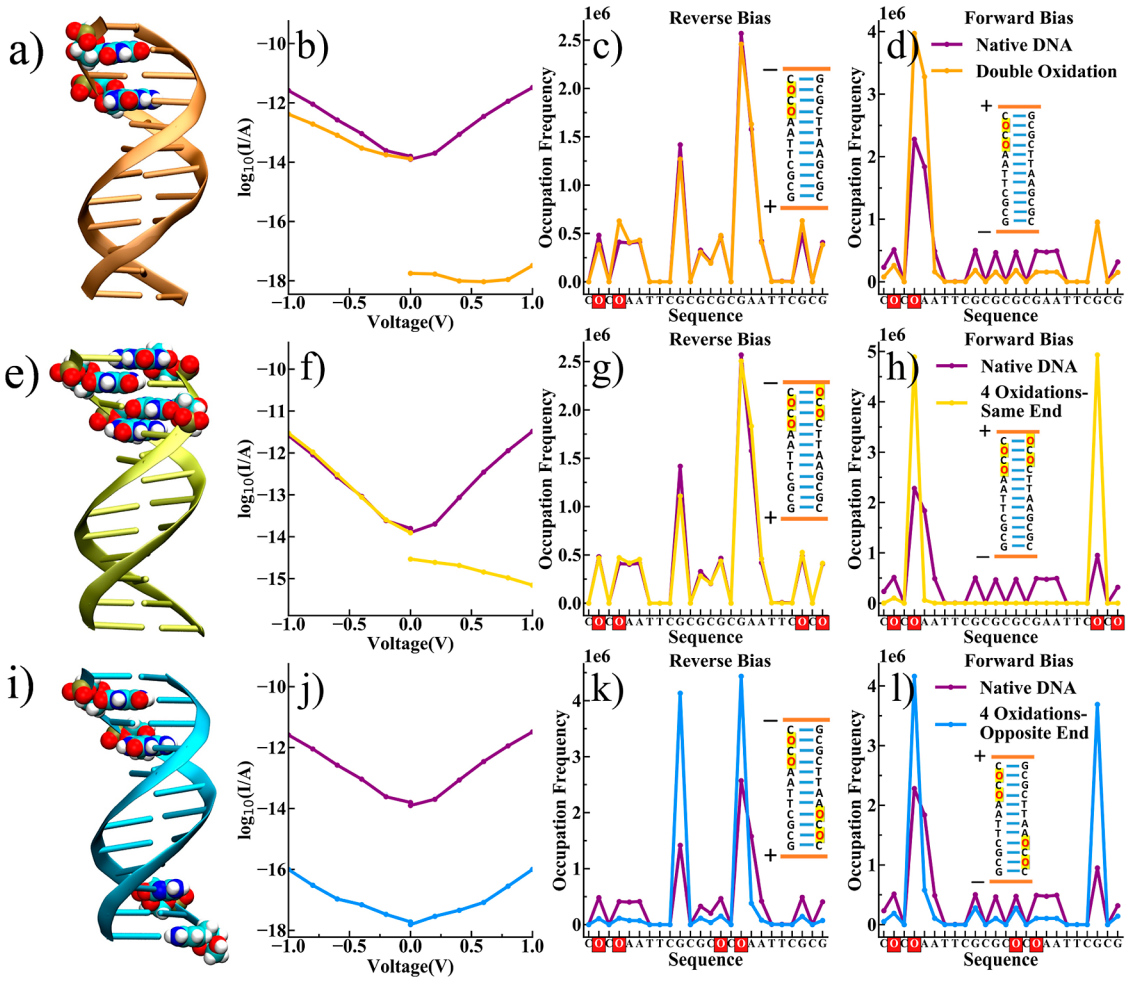

Figure 4. Effect of double and quadruple guanine oxidations on CT properties of Drew−Dickerson dsDNA. (a) 3-D structure of double-oxidized Drew−Dickerson dsDNA at the 2nd and 4th sites. 8oxoG is shown in a VDW representation. (b) *I*−*V* characteristics of the double-oxidized dsDNA. The occupation frequency of the charge during the KMC simulations for (c) reverse bias and (d) forward bias for double oxidation. (e) 3-D structure of quadruple-oxidized Drew−Dickerson dsDNA at the same end. (f) *I*−*V* characteristics and the occupation frequency of the charge during the KMC simulations for (g) reverse bias and (h) forward bias for quadruple oxidation at the same end. (i) 3-D structure of quadruple-oxidized Drew−Dickerson dsDNA at opposite ends. (f) *I*−*V* characteristics and the occupation frequency of the charge during the KMC simulations for (g) reverse bias and (h) forward bias for quadruple oxidation at opposite ends.

This signifies a 6 order of magnitude rectification in the double oxidation case of the Drew−Dickerson sequence. A sharp spike in the occurrence frequency in the forward bias in double-oxidized dsDNA marks the trapping of charge on 8oxoG sites. However, the two sequences qualitatively have similar *I*−*V* characteristics for the reverse bias. This is because of the asymmetry in the sequence, which results in higher energy differences in the forward bias, as the site energy difference increases in the direction of flow of charge. The high RR of around 3 orders of magnitude makes such dsDNA sequences perfect candidates for molecular switches.

Next, we replace four guanine bases of the two strands at the same end with 8oxoG bases in one case (Figure 4e) and opposite ends in the other (Figure 4i). In the quadruple oxidation at the same end, the *I*−*V* characteristics signify that the oxidized dsDNA sequence shows a rectifying behavior with a high RR of 2.3×10^{-4}. In the forward bias, the charge gets trapped on the two oxidized guanines, as evident in Figure 4g, and cannot traverse through these oxidized guanines because of the vast energy difference. In reverse bias, as a voltage is applied at the end of the DNA sequence having normal guanine bases, the energy disparity between the oxidized guanines in the two strands decreases. Therefore, the *I*−*V* characteristics of the native and oxidized DNA are similar in the reverse bias.

In quadruple oxidation at opposite ends, the dsDNA conductance decreases up to 2 orders of magnitude upon oxidation in both forward and reverse biases. This is because of the trapping of charge at the oxidized guanines in both reverse (Figure 4k) and forward (Figure 4l) bias conditions. However, as both the 5′−3′ strands of the dsDNA sequence are symmetric to each other in this case, no rectification behavior is seen.

Finally, we study the Drew−Dickerson sequence with all the guanine bases oxidized to 8oxoG (Figure 5). We find that the conductance decreases by an order of magnitude and the trapping of charge at the oxidized guanine sites is higher compared to the native dsDNA (Figure 5a). Notably, since the sequence is completely symmetric in this case, the charge gets highly trapped on the 8oxoG sites. It is noteworthy to mention here that the charge gets trapped in the same guanine locations

https://doi.org/10.1021/acs.jpcb.2c01371
J. Phys. Chem. B 2022, 126, 4636−4646

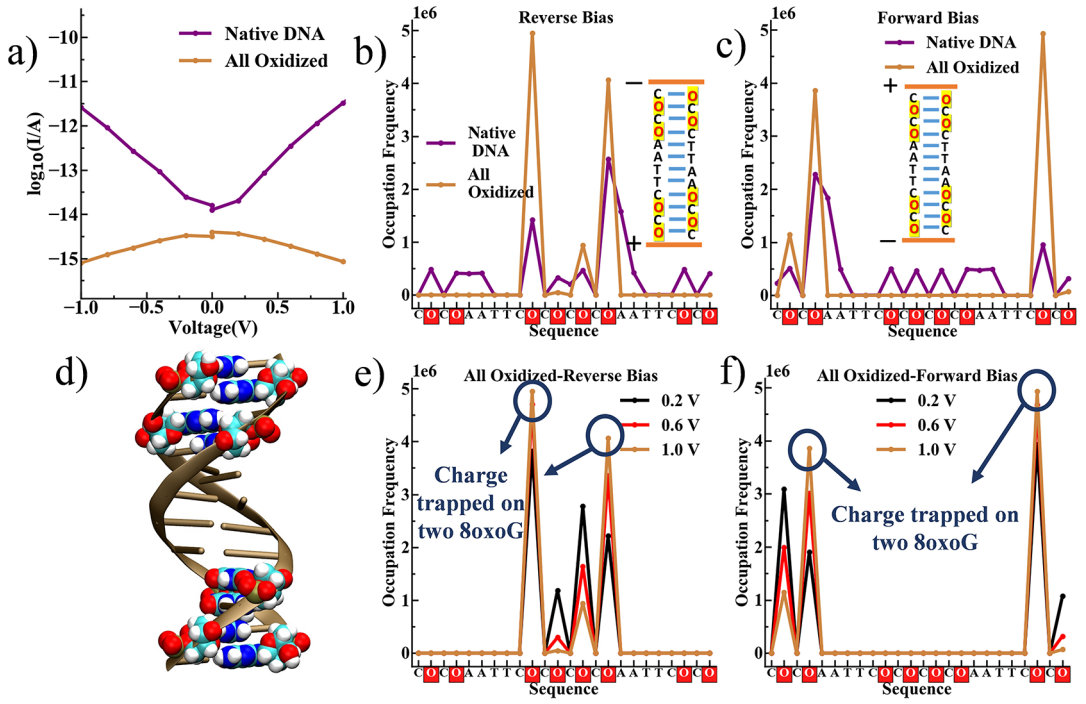

Figure 5. Effect of replacing all guanines of the Drew−Dickerson sequence with 8oxoG on its CT properties. (a) *I*−*V* characteristics of the native Drew−Dickerson sequence compared to that of oxidized dsDNA with all the guanines replaced with 8oxoG. The occupation frequency of the charge during the KMC simulations for (b) reverse bias and (c) forward bias. (d) 3-D structure of the Drew−Dickerson dsDNA sequence with all the guanines oxidized. The 8oxoGs are shown in a VDW representation. The variation of the occupation frequency for different applied voltages in (e) reverse bias and (f) forward bias. Clearly, as the voltage increases, the charge gets more and more trapped on the two 8oxoGs in all-oxidized dsDNA, leading to NDR phenomena.

in the sequence, where the occupation frequency was higher in the native dsDNA case as well (Figure 5b,c).

In Figure 5a, one can clearly see that the conductance of the fully oxidized Drew−Dickerson sequence shows traits of NDR, that is, the conductance decreases with increasing voltage. To understand the reason behind this observation, we present the occupation frequency graph at different applied potential in reverse bias (Figure 5e) and forward bias (Figure 5f). We see that as the voltage increases, the charge gets more and more trapped on two 8oxoGs in both the biases. This is because as the potential bias increases, the difference between the site energies of 8oxoG and other nucleobases increases, and the charge has nowhere to escape than getting trapped at two 8oxoGs. Similar traits of NDR can be seen in the forward bias configuration of quadruple oxidation at the same end (Figure 4f). Here as well, as seen in Figure 4h, the charge gets trapped at two 8oxoGs, which increases as the potential bias increases. Thus, a complete understanding of the flow of charge in dsDNA molecules can be made by analyzing the charge dynamics. This provides a unique tool to control/tune the flow of charge in a dsDNA sequence.

In this work, we have discussed and proposed the potential of using oxidized dsDNA in molecular electronics applications. We have first presented the *I*−*V* characteristic curves for the 12 bp poly-G dsDNA sequence having different concentrations of 8oxoGs at different locations of dsDNA. We see that the dsDNA conductance decreases upon oxidation (Figure 2), which is explained based on the larger reorganization energy and site energy differences required for the charge hopping from 8oxoG relative to native guanine (Table 1). To harness this understanding in building molecular electronic devices, we study different cases where we replace various native guanines of the Drew−Dickerson sequence with 8oxoG. When a single guanine is replaced with 8oxoG, we find that oxidized dsDNA shows rectifying properties due to the asymmetry induced in the dsDNA structure upon oxidation (Figure 3). This is evidenced by the occurrence frequency plots where we observe that the charge gets trapped at the oxidized site when the electrode is closer to the oxidation site. When two guanines in the Drew−Dickerson sequence are replaced by 8oxoG, we see similar rectifying properties (Figure 4a−h). However, when the dsDNA is symmetrically oxidized with four guanines, we do not see any rectification behavior. However, a significant decrease in conductance is observed in this case (Figure 4j). Interestingly, when all the guanines of the Drew−Dickerson sequence are oxidized, we find that dsDNA shows a NDR effect; that is, the current decreases as the voltage increases. This is because of the complete trapping of charge at 8oxoG in this case (Figure 5). Thus, in this work, we have presented a unique tool to control/tune the flow of charge in a dsDNA sequence.

CONCLUSIONS

In conclusion, we have presented a novel strategy to construct a molecular rectifier with record RR of 10^6 using oxidatively damaged dsDNA molecules. The ability to harness the power of rectifying ability of oxidized dsDNA opens doors to numerous practical applications such as molecular switches, bioelectronic sensors, molecular diodes, and so on. Using a multiscale methodology that combines MD, DFT, and KMC simulations, we find that an oxidized guanine acts as a charge trapping barrier, leading to lesser electronic conduction in oxidized dsDNA relative to the corresponding native dsDNA. This work provides a fundamental understanding of the charge

https://doi.org/10.1021/acs.jpcb.2c01371
J. Phys. Chem. B 2022, 126, 4636−4646

dynamics in oxidatively damaged dsDNA sequences and a novel strategy to use DNA molecules in electronic applications. This study will motivate further experimental works to explore the tunable rectifying properties of DNA using state-of-the-art single-molecule experimental techniques[72] such as scanning tunneling microscopy break junction (STM-BJ) and mechanically controllable break junction (MCBJ) setups. Having a huge biological significance, an elementary understanding of the CT processes in oxidized dsDNA is essential to study their role in countless cell functions and will ultimately aid to cure numerous diseases.

AUTHOR INFORMATION

Corresponding Author

Prabal K. Maiti − *Center for Condensed Matter Theory, Department of Physics, Indian Institute of Science, Bangalore 560012, India;* orcid.org/0000-0002-9956-1136; Email: maiti@iisc.ac.in

Authors

Abhishek Aggarwal − *Center for Condensed Matter Theory, Department of Physics, Indian Institute of Science, Bangalore 560012, India;* orcid.org/0000-0002-3342-6484

Supriyo Naskar − *Center for Condensed Matter Theory, Department of Physics, Indian Institute of Science, Bangalore 560012, India;* orcid.org/0000-0002-3690-6483

Complete contact information is available at: https://pubs.acs.org/10.1021/acs.jpcb.2c01371

Notes

The authors declare no competing financial interest.

ACKNOWLEDGMENTS

A.A. and S.N. thank the MHRD, India, and CSIR, India, respectively, for the research fellowship. The authors also acknowledge the DST, India, for the computational support through the TUE-CMS machine, IISc.

REFERENCES

(1) Nozaki, D.; Lokamani; Santana-Bonilla, A.; Dianat, A.; Gutierrez, R.; Cuniberti, G. Switchable Negative Differential Resistance Induced by Quantum Interference Effects in Porphyrin-Based Molecular Junctions. *J. Phys. Chem. Lett.* **2015**, *6*, 3950−3955.

(2) Hettler, M. H.; Schoeller, H.; Wenzel, W. Non-Linear Transport through a Molecular Nanojunction. *Europhys. Lett.* **2002**, *57*, 571.

(3) Yuan, L.; Breuer, R.; Jiang, L.; Schmittel, M.; Nijhuis, C. A. A Molecular Diode with a Statistically Robust Rectification Ratio of Three Orders of Magnitude. *Nano Lett.* **2015**, *15*, 5506−5512.

(4) Chen, X.; Roemer, M.; Yuan, L.; Du, W.; Thompson, D.; del Barco, E.; Nijhuis, C. A. Molecular Diodes with Rectification Ratios Exceeding 105 Driven by Electrostatic Interactions. *Nat. Nanotechnol.* **2017**, *12*, 797−803.

(5) Aggarwal, A.; Kaliginedi, V.; Maiti, P. K. Quantum Circuit Rules for Molecular Electronic Systems: Where Are We Headed Based on the Current Understanding of Quantum Interference, Thermoelectric, and Molecular Spintronics Phenomena? *Nano Lett.* **2021**, *21*, 8532−8544.

(6) Ke, S.-H.; Yang, W.; Baranger, H. U. Quantum-Interference-Controlled Molecular Electronics. *Nano Lett.* **2008**, *8*, 3257−3261.

(7) Aviram, A.; Ratner, M. A. Molecular Rectifiers. *Chem. Phys. Lett.* **1974**, *29*, 277−283.

(8) Valdiviezo, J.; Palma, J. L. Molecular Rectification Enhancement Based On Conformational and Chemical Modifications. *J. Phys. Chem. C* **2018**, *122*, 2053−2063.

(9) Guo, C.; Wang, K.; Zerah-Harush, E.; Hamill, J.; Wang, B.; Dubi, Y.; Xu, B. Molecular Rectifier Composed of DNA with High Rectification Ratio Enabled by Intercalation. *Nat. Chem.* **2016**, *8*, 484−490.

(10) Tsuji, Y.; Staykov, A.; Yoshizawa, K. Molecular Rectifier Based on π-π Stacked Charge Transfer Complex. *J. Phys. Chem. C* **2012**, *116*, 2575−2580.

(11) Martin, A. S.; Sambles, J. R.; Ashwell, G. J. Molecular rectifier. *Phys. Rev. Lett.* **1993**, *70*, 218−221.

(12) Elbing, M.; Ochs, R.; Koentopp, M.; Fischer, M.; von Hänisch, C.; Weigend, F.; Evers, F.; Weber, H. B.; Mayor, M. A Single-Molecule Diode. *Proc. Natl. Acad. Sci. U. S. A.* **2005**, *102*, 8815−8820.

(13) Batra, A.; Darancet, P.; Chen, Q.; Meisner, J. S.; Widawsky, J. R.; Neaton, J. B.; Nuckolls, C.; Venkataraman, L. Tuning Rectification in Single-Molecular Diodes. *Nano Lett.* **2013**, *13*, 6233−6237.

(14) Wang, K.; Zhou, J.; Hamill, J. M.; Xu, B. Measurement and Understanding of Single-Molecule Break Junction Rectification Caused by Asymmetric Contacts. *J. Chem. Phys.* **2014**, *141*, 054712.

(15) Capozzi, B.; Xia, J.; Adak, O.; Dell, E. J.; Liu, Z.-F.; Taylor, J. C.; Neaton, J. B.; Campos, L. M.; Venkataraman, L. Single-Molecule Diodes with High Rectification Ratios through Environmental Control. *Nat. Nanotechnol.* **2015**, *10*, 522−527.

(16) Li, Y.; Artés, J. M.; Demir, B.; Gokce, S.; Mohammad, H. M.; Alangari, M.; Anantram, M. P.; Oren, E. E.; Hihath, J. Detection and Identification of Genetic Material via Single-Molecule Conductance. *Nat. Nanotechnol.* **2018**, *13*, 1167−1173.

(17) Artés, J. M.; Li, Y.; Qi, J.; Anantram, M. P.; Hihath, J. Conformational Gating of DNA Conductance. *Nat. Commun.* **2015**, *6*, 8870.

(18) Aggarwal, A.; Bag, S.; Maiti, P. K. Remarkable Similarity of Force Induced DsRNA Conformational Changes to Stretched DsDNA and Their Detection Using Electrical Measurements. *Phys. Chem. Chem. Phys.* **2018**, *20*, 28920−28928.

(19) Aggarwal, A.; Naskar, S.; Sahoo, A. K.; Mogurampelly, S.; Garai, A.; Maiti, P. K. What Do We Know about DNA Mechanics so Far? *Curr. Opin. Struct. Biol.* **2020**, *64*, 42−50.

(20) Aggarwal, A.; Bag, S.; Venkatramani, R.; Jain, M.; Maiti, P. K. Multiscale Modelling Reveals Higher Charge Transport Efficiencies of DNA Relative to RNA Independent of Mechanism. *Nanoscale* **2020**, *12*, 18750−18760.

(21) Genereux, J. C.; Barton, J. K. Mechanisms for DNA Charge Transport. *Chem. Rev.* **2010**, *110*, 1642−1662.

(22) Venkatramani, R.; Keinan, S.; Balaeff, A.; Beratan, D. N. Nucleic Acid Charge Transfer: Black, White and Gray. *Coord. Chem. Rev.* **2011**, *255*, 635−648.

(23) Wang, K. DNA-Based Single-Molecule Electronics: From Concept to Function. *J. Funct. Biomater.* **2018**, *9*, 8.

(24) Valdiviezo, J.; Clever, C.; Beall, E.; Pearse, A.; Bae, Y.; Zhang, P.; Achim, C.; Beratan, D. N.; Waldeck, D. H. Delocalization-Assisted Transport through Nucleic Acids in Molecular Junctions. *Biochemistry* **2021**, *60*, 1368−1378.

(25) Aggarwal, A.; Sahoo, A. K.; Bag, S.; Kaliginedi, V.; Jain, M.; Maiti, P. K. Fine-Tuning the DNA Conductance by Intercalation of Drug Molecules. *Phys. Rev. E* **2021**, *103*, 032411.

(26) Mallajosyula, S. S.; Pati, S. K. Toward DNA Conductivity: A Theoretical Perspective. *J. Phys. Chem. Lett.* **2010**, *1*, 1881−1894.

(27) Troisi, A.; Orlandi, G. Hole Migration in DNA: A Theoretical Analysis of the Role of Structural Fluctuations. *J. Phys. Chem. B* **2002**, *106*, 2093−2101.

(28) van Zalinge, H.; Schiffrin, D. J.; Bates, A. D.; Starikov, E. B.; Wenzel, W.; Nichols, R. J.; van Zalinge, H.; Schiffrin, D. J.; Nichols, R. J.; Bates, A. D.; Starikov, E. B.; Wenzel, W. Variable-Temperature Measurements of the Single-Molecule Conductance of Double-Stranded DNA. *Angew. Chem., Int. Ed.* **2006**, *45*, 5499−5502.

(29) Narayanaswamy, N.; Das, S.; Samanta, P. K.; Banu, K.; Sharma, G. P.; Mondal, N.; Dhar, S. K.; Pati, S. K.; Govindaraju, T. Sequence-Specific Recognition of DNA Minor Groove by an NIR-Fluorescence Switch-on Probe and Its Potential Applications. *Nucleic Acids Res.* **2015**, *43*, 8651−8663.

(30) Aggarwal, A.; Vinayak, V.; Bag, S.; Bhattacharyya, C.; Waghmare, U. v.; Maiti, P. K. Predicting the DNA Conductance Using a Deep Feedforward Neural Network Model. *J. Chem. Inf. Model.* **2021**, *61*, 106−114.
(31) Sosorev, A.; Kharlanov, O. Organic Nanoelectronics inside Us: Charge Transport and Localization in RNA Could Orchestrate Ribosome Operation. *Phys. Chem. Chem. Phys.* **2021**, *23*, 7037−7047.
(32) Cooke, M. S.; Evans, M. D.; Dizdaroglu, M.; Lunec, J. Oxidative DNA Damage: Mechanisms, Mutation, and Disease. *Faseb. J.* **2003**, *17*, 1195−1214.
(33) Diamantis, P.; Tavernelli, I.; Rothlisberger, U. Redox Properties of Native and Damaged DNA from Mixed Quantum Mechanical/Molecular Mechanics Molecular Dynamics Simulations. *J. Chem. Theory Comput.* **2020**, *16*, 6690−6701.
(34) Gattuso, H.; Durand, E.; Bignon, E.; Morell, C.; Georgakilas, A. G.; Dumont, E.; Chipot, C.; Dehez, F.; Monari, A. Repair Rate of Clustered Abasic DNA Lesions by Human Endonuclease: Molecular Bases of Sequence Specificity. *J. Phys. Chem. Lett.* **2016**, *7*, 3760−3765.
(35) Lu, A. L.; Clark, S.; Modrich, P. Methyl-Directed Repair of DNA Base-Pair Mismatches in Vitro. *Proc. Natl. Acad. Sci. U.S.A.* **1983**, *80*, 4639−4643.
(36) Iyer, R. R.; Pluciennik, A.; Burdett, V.; Modrich, P. L. DNA Mismatch Repair: Functions and Mechanisms. *Chem. Rev.* **2005**, *106*, 302−323.
(37) Reardon, J. T.; Sancar, A. Recognition and Repair of the Cyclobutane Thymine Dimer, a Major Cause of Skin Cancers, by the Human Excision Nuclease. *Genes Dev.* **2003**, *17*, 2539−2551.
(38) van Loon, B.; Markkanen, E.; Hübscher, U. Oxygen as a Friend and Enemy: How to Combat the Mutational Potential of 8-Oxo-Guanine. *DNA Repair*; Elsevier, 2010; Vol. *9*, pp 604−616.
(39) Nogueira, J. J.; Plasser, F.; González, L. Electronic Delocalization, Charge Transfer and Hypochromism in the UV Absorption Spectrum of Polyadenine Unravelled by Multiscale Computations and Quantitative Wavefunction Analysis. *Chem. Sci.* **2017**, *8*, 5682−5691.
(40) Szabla, R.; Zdrowowicz, M.; Spisz, P.; Green, N. J.; Stadlbauer, P.; Kruse, H.; Šponer, J.; Rak, J. 2,6-Diaminopurine Promotes Repair of DNA Lesions under Prebiotic Conditions. *Nat. Commun.* **2021**, *12*, 1−11.
(41) Nguyen, K. V.; Burrows, C. J. A Prebiotic Role for 8-Oxoguanosine as a Flavin Mimic in Pyrimidine Dimer Photorepair. *J. Am. Chem. Soc.* **2011**, *133*, 14586−14589.
(42) Lee, W.; Matsika, S. Role of Charge Transfer States into the Formation of Cyclobutane Pyrimidine Dimers in DNA. *Faraday Discuss.* **2019**, *216*, 507−519.
(43) Diamantis, P.; Tavernelli, I.; Rothlisberger, U. Vertical Ionization Energies and Electron Affinities of Native and Damaged DNA Bases, Nucleotides, and Pairs from Density Functional Theory Calculations: Model Assessment and Implications for DNA Damage Recognition and Repair. *J. Chem. Theory Comput.* **2019**, *15*, 2042−2052.
(44) Prat, F.; Houk, K. N.; Foote, C. S. Effect of Guanine Stacking on the Oxidation of 8-Oxoguanine in B-DNA. *J. Am. Chem. Soc.* **1998**, *120*, 845−846.
(45) Mishra, S.; Poonia, V. S.; Fontanesi, C.; Naaman, R.; Fleming, A. M.; Burrows, C. J. Effect of Oxidative Damage on Charge and Spin Transport in DNA. *J. Am. Chem. Soc.* **2019**, *141*, 123−126.
(46) Markus, T. Z.; Daube, S. S.; Naaman, R.; Fleming, A. M.; Muller, J. G.; Burrows, C. J. Electronic Structure of DNA - Unique Properties of 8-Oxoguanosine. *J. Am. Chem. Soc.* **2009**, *131*, 89−95.
(47) Lee, M. H.; Brancolini, G.; Gutiérrez, R.; di Felice, R.; Cuniberti, G. Probing Charge Transport in Oxidatively Damaged DNA Sequences under the Influence of Structural Fluctuations. *J. Phys. Chem. B* **2012**, *116*, 10977−10985.
(48) Jang, Y. H.; Goddard, W. A.; Noyes, K. T.; Sowers, L. C.; Hwang, S.; Chung, D. S. First Principles Calculations of the Tautomers and PKa Values of 8-Oxoguanine: Implications for Mutagenicity and Repair. *Chem. Res. Toxicol.* **2002**, *15*, 1023−1035.
(49) Boon, E. M.; Livingston, A. L.; Chmiel, N. H.; David, S. S.; Barton, J. K. DNA-Mediated Charge Transport for DNA Repair. *Proc. Natl. Acad. Sci. U. S. A.* **2003**, *100*, 12543−12547.
(50) Odom, D. T.; Barton, J. K. Long-Range Oxidative Damage in DNA/RNA Duplexes. *Biochemistry* **2001**, *40*, 8727−8737.
(51) Bag, S.; Aggarwal, A.; Maiti, P. K. Machine Learning Prediction of Electronic Coupling between the Guanine Bases of DNA. *J. Phys. Chem. A* **2020**, *124*, 7658−7664.
(52) Wolter, M.; Elstner, M.; Kubař, T. Charge Transport in Desolvated DNA. *J. Chem. Phys.* **2013**, *139*, 125102.
(53) Bag, S.; Biswas, T.; Jain, M.; Maiti, P. K. Anisotropic Charge Transport in Nanoscale DNA Wire. *J. Phys. Chem. C* **2020**, *124*, 16763−16772.
(54) Rühle, V.; Lukyanov, A.; May, F.; Schrader, M.; Vehoff, T.; Kirkpatrick, J.; Baumeier, B.; Andrienko, D. Microscopic Simulations of Charge Transport in Disordered Organic Semiconductors. *J. Chem. Theory Comput.* **2011**, *7*, 3335−3345.
(55) Case, D. A.; Cheatham, T. E.; Darden, T.; Gohlke, H.; Luo, R.; Merz, K. M.; Onufriev, A.; Simmerling, C.; Wang, B.; Woods, R. J. The Amber Biomolecular Simulation Programs. *J. Comput. Chem.* **2005**, *26*, 1668−1688.
(56) Macpherson, P.; Barone, F.; Maga, G.; Mazzei, F.; Karran, P.; Bignami, M. 8-Oxoguanine incorporation into DNA repeats in vitro and mismatch recognition by MutS. *Nucleic Acids Res.* **2005**, *33*, 5094.
(57) Sugden, K. D.; Campo, C. K.; Martin, B. D. Direct Oxidation of Guanine and 7,8-Dihydro-8-Oxoguanine in DNA by a High-Valent Chromium Complex: A Possible Mechanism for Chromate Genotoxicity. *Chem. Res. Toxicol.* **2001**, *14*, 1315−1322.
(58) Case, D. A.; Cheatham, T. E.; Darden, T.; Gohlke, H.; Luo, R.; Merz, K. M.; Onufriev, A.; Simmerling, C.; Wang, B.; Woods, R. J. The Amber Biomolecular Simulation Programs. *J. Comput. Chem.* **2005**, *26*, 1668−1688.
(59) Miller, J. H.; Fan-Chiang, C.-C. P.; Straatsma, T. P.; Kennedy, M. A. 8-Oxoguanine Enhances Bending of DNA that Favors Binding to Glycosylases. *J. Am. Chem. Soc.* **2003**, *125*, 6331−6336.
(60) Jorgensen, W. L.; Chandrasekhar, J.; Madura, J. D.; Impey, R. W.; Klein, M. L. Comparison of Simple Potential Functions for Simulating Liquid Water. *J. Chem. Phys.* **1983**, *79*, 926.
(61) Joung, I. S.; Cheatham, T. E. Determination of Alkali and Halide Monovalent Ion Parameters for Use in Explicitly Solvated Biomolecular Simulations. *J. Phys. Chem. B* **2008**, *112*, 9020−9041.
(62) Darden, T.; York, D.; Pedersen, L. Particle mesh Ewald: AnN·log(N) method for Ewald sums in large systems. *J. Chem. Phys.* **1993**, *98*, 10089−10092.
(63) Marcus, R. A. Electron Transfer Reactions in Chemistry. Theory and Experiment. *Rev. Mod. Phys.* **1993**, *65*, 599−610.
(64) Endres, R. G.; Cox, D. L.; Singh, R. R. P. Colloquium: The Quest for High-Conductance DNA. *Rev. Mod. Phys.* **2004**, *76*, 195−214.
(65) Tomasi, J.; Mennucci, B.; Cammi, R. Quantum Mechanical Continuum Solvation Models. *Chemical Reviews*; American Chemical Society, 2005, Vol *105*, pp 2999−3094.
(66) Kubař, T.; Elstner, M. What Governs the Charge Transfer in DNA? The Role of DNA Conformation and Environment. *J. Phys. Chem. B* **2008**, *112*, 8788−8798.
(67) Woiczikowski, P. B.; Steinbrecher, T.; Kubař, T.; Elstner, M. Nonadiabatic QM/MM Simulations of Fast Charge Transfer in Escherichia Coli DNA Photolyase. *J. Phys. Chem. B* **2011**, *115*, 9846−9863.
(68) Pluhařová, E.; Slavíček, P.; Jungwirth, P. Modeling Photoionization of Aqueous DNA and Its Components. *Acc. Chem. Res.* **2015**, *48*, 1209−1217.
(69) Pliego, J. R.; Riveros, J. M. Theoretical Calculation of pKa Using the Cluster−Continuum Model. *J. Phys. Chem. A* **2002**, *106*, 7434−7439.
(70) Gasper, S. M.; Schuster, G. B. Intramolecular Photoinduced Electron Transfer to Anthraquinones Linked to Duplex DNA: The Effect of Gaps and Traps on Long-Range Radical Cation Migration. *J. Am. Chem. Soc.* **1997**, *119*, 12762−12771.

https://doi.org/10.1021/acs.jpcb.2c01371
J. Phys. Chem. B 2022, 126, 4636−4646

(71) Heller, A. Spiers Memorial Lecture: On the hypothesis of cathodic protection of genes. *Faraday Discuss.* **2000**, *116*, 1−13.
(72) Fu, T.; Frommer, K.; Nuckolls, C.; Venkataraman, L. Single-Molecule Junction Formation in Break-Junction Measurements. *J. Phys. Chem. Lett.* **2021**, *12*, 10802−10807.

https://doi.org/10.1021/acs.jpcb.2c01371
J. Phys. Chem. B 2022, 126, 4636−4646